On The Theoretical Limits of The Power Efficiency of Photonically Generated IR-UWB Waveforms

Mohamed Shehata, *Member, IEEE,* Hassan Mostafa, *Senior Member, IEEE,* and Yehea Ismail, *Fellow, IEEE*

***Abstract*—The design and photonic generation of power efficient impulse radio ultra wideband (IR-UWB) waveforms is a challenging step in the design and development of IR-UWB over fiber (IR-UWBoF) systems with combined optical and wireless transmission. In this paper, the definition of the spectral power efficiency (SPE) and its associated optimization problem are reformulated. Based on this reformulation, a theoretical upper bound for the SPE is derived and applied to two of the most common types of photonically generated IR-UWB waveforms. Accurate closed form analytical expressions for the SPE upper bounds of these two waveform types are obtained and optimized. The analytical framework presented in this work can be extended and applied to other waveform types. Simulation results show excellent agreement with the analytically obtained expressions. Accordingly, these analytical expressions can be used as reliable guidelines for precise and efficient design of practical IR-UWBoF systems that guarantee optimal design, generation and distribution of IR-UWB waveforms.**

***Index Terms*—Impulse radio (IR), microwave photonic (MWP), spectral power efficiency (SPE), ultra wideband over fiber (UWBoF).**

I. Introduction

IN THE PAST decade, the US Federal Communications Committee (FCC) has dedicated a very wide bandwidth, called the useful UWB band and ranges from 3.1 GHz to 10.6 GHz, for indoor UWB signalling. However, the maximum effective isotropic radiation power (EIRP) spectral density has been restricted to only -41.3 dBm/MHz [1]. A UWB signal that fully occupies the useful UWB band with the maximum admissible PSD possesses a total EIRP of only about 0.56 mW. In IR-UWB signalling, such extremely low power is emitted to the wireless channel in the form of energy bursts, carried by ultrashort (ns∼ps) baseband waveforms. The PSD of a UWB signal should be carefully reshaped and theoretically optimized *a priori* in the design and development of practical IR-UWB over fiber (IR-UWBoF) systems with combined optical and wireless transmission in a way such that optimal IR-UWB waveforms (i.e., with the highest possible SPE, subject to the FCC spectral constrains) are guaranteed at each point along the IR-UWBoF transceiver chain.

M. Shehata and H. Mostafa are with the Opto Nano Electronics (ONE) Laboratory in the Department of Electrical Engineering, Cairo University, Giza 12613, Egypt, e-mail: (m.shehata_ieee@yahoo.com , hmostafa@uwaterloo.ca).

H. Mostafa and Y. Ismail are with the Nanotechnology program at Zewail City for Science and technology, Giza 12588, Egypt. email: (hmostafa@zewailcity.edu.eg, y.ismail@aucegypt.edu).

Manuscript received Month xx, 2017; revised Month xx, 2017; accepted Month xx, 2017. Date of publication Month xx, 2017; date of current version Month xx, 2017. This work was supported by the national telecommunications regulatory authority of Egypt (NTRA-Egypt), and in part by MCIT.

According to [2], the spectrum of an IR-UWB signal is reshaped by using one or more of three possible techniques, namely, differentiating the baseband IR-UWB waveform, varying its pulse width and/or combination of these two operations. Several approaches have been reported to demonstrate the design and/or optical generation of IR-UWB waveforms using one or more of these three techniques [3]-[9]. Unfortunately, the reported techniques focus only on the design and/or implementation of the optical generation process to produce the desired IR-UWB waveform, while ignoring the SPE of the resulting waveform. Only few of the reported techniques (e.g., [10]) follow a deterministic approach to maximize the SPE of the photonically generated IR-UWB waveform. However, the impact of optical and/or wireless transmission on the SPE of the resulting waveform is not considered. To the best of the authors' knowledge, no study has been reported to assess the limits of the SPE of photonically generated IR-UWB waveforms in IR-UWBoF systems with combined optical and wireless transmission under the FCC spectral constraints. Inspired by the hybrid theoretical/experimental approaches provided in [11],[12] for the design and photonic generation of IR-UWB waveforms, an analytical disjoint optimization approach is proposed to maximize the SPE of a photonically generated IR-UWB waveform resulting from an arbitrary IR-UWBoF system with combined optical and wireless transmission, subject to the FCC spectral constraints.

The rest of the paper is organized as follows. In Section II, a typical and comprehensive architecture of IR-UWBoF systems is overviewed and modelled from a frequency domain perspective. In Section III, the SPE optimization problem is reformulated and applied to Gaussian and soliton-based IR-UWB waveforms. Theoretical expressions for the SPE upper bound of these two waveform types are obtained. Section IV presents numerical results which validate the analytical expressions obtained in Section III. The whole paper is finally concluded in Section VII.

II. System Model Overview

A typical unidirectional IR-UWBoF system with combined optical and wireless transmission chains is shown in Fig. 1. Clearly, the system consists of two main parts. The first part is the combination of the optical source(s), the optical modulator (OM), the microwave photonic (MWP) filter and the single mode fiber (SMF), that forms the optical microwave photonic processing (MWPP), and the optical transmission chain of the IR-UWBoF system. Whereas the second part consists of the power amplifier (PA), the UWB TX antenna, the UWB wireless channel, the UWB RX antenna, the low

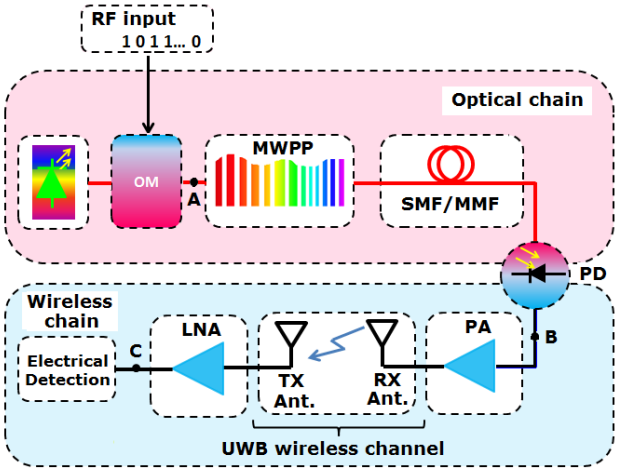

Fig. 1. Schematic architecture of a typical IR-UWBoF system with combined optical and wireless transmission. OM: optical modulator. MWPP: microwave photonic processing. SMF: single mode fiber. MMF: multimode fiber. PD: photodetector. PA: power amplifier. LNA: low noise amplifier. Red lines: optical paths. Black lines: electrical paths.

noise amplifier (LNA) and the electrical UWB receiver. The components of the second part form the wireless transmission and processing chain. Both chains are coupled via a high speed photodetector (PD).

The entire system is driven by an RF signal that modulates either a pulsed or a continuous wave (CW) optical carrier. The resulting modulated optical carrier is forwarded to the MWP filter for further optical processing. In the MWP filter, various optical phenomena exhibited by different MWP components are utilized to implement one or more communication processing functions in the optical domain such as optical pulse shaping and higher order modulation. The detailed architecture, the principle of operation, the modelling, and the implementation complexity of the MWP filter depend on the characteristics of the components utilized to implement a particular photonic generation approach.

The photonically generated and encoded IR-UWB waveform is then coupled to an optical fiber link, usually a linear dispersive SMF, that performs two typical operations. The first operation is that the SMF works as an optical transmission medium to an access point at a remote location, up to several tens of kilometers away from the central station. The second operation is that the SMF is also used as a part of the photonic generation process. For example, the SMF is used as a dispersive element in case of frequency to time mapping [13]. At the output end of the SMF, a PD stage is necessary to transform the received optical signal back to the electrical domain. The power of the RF signal at the PD output is boosted by a radio frequency PA before being radiated to the UWB wireless channel via a UWB TX antenna. The radiated RF signal is received by a remote UWB RX antenna which is few meters distance apart from the UWB TX antenna. The weak power of the received IR-UWB signal is boosted by an LNA before being passed to an electrical UWB receiver for further electrical processing and detection of information symbols.

A. Basis Functions of IR-UWB Waveforms

In the literature reported on IR-UWBoF systems, the Gaussian [14] and the hyperbolic secant (sech) [15] pulses are the conventional basis functions from which IR-UWB monocycles, doublets and higher order derivatives are generated. At the OM output (Point A in Fig. 1), an optical pulse with a Gaussian profile best approximates the waveform resulting from impressing a high-speed electronically switched rectangular waveform on a constant power continuous wave (CW) optical carrier [16]. However, such switched rectangular pulse appears as essentially flat with respect to an ultra-short optical pulse produced by a pulsed optical source such as a mode locked fiber laser (MLFL), whose profile is best approximated by an ideal sech pulse, commonly called a soliton. From a mathematical perspective, the optical electric field envelope resulting from either approach at Point A in Fig. 1 is equivalent and is represented as an optical input basis function $\psi(t/\tau)$ repeated every T_s seconds. This equivalence principle is illustrated in Fig. 2 (a) as a block diagram representation of the OM. The modulated optical electric field $E(t)$ at point A in Figs. 1 and 2 is expressed as follows:

$$E(t) = \sqrt{2P_o}\left(\sum_{i=-\infty}^{+\infty} \psi(t/\tau - iT_s)\right)\exp(j2\pi c/\lambda_o t) \quad (1)$$

where P_o is the power emitted by the optical source, λ_o is its central emission wavelength and $\psi(t/\tau)$ is given by

$$\underset{-T_s/2\leq t\leq T_s/2}{\psi(t/\tau)} = \begin{cases} \exp(-t^2/{\tau_g}^2); & \text{for Gaussian input} \\ sech(t/\tau_s); & \text{for soliton input} \end{cases} \quad (2)$$

where τ_g is the Gaussian pulse width defined as the e^{-1} point of the magnitude profile of the input Gaussian pulse, τ_s is the soliton pulse width defined as the point at which the magnitude profile of the soliton pulse decreases to about 65% of its maximum value and τ is the full width at half maximum (FWHM) pulse width and is common to both types of input basis functions. The FWHM pulse width of the input basis function is related to the Gaussian and soliton pulse widths as $\tau = 2\sqrt{-\log(1/2)}\tau_g$ and $\tau = 2sech^{-1}(1/2)\tau_s$, respectively.

B. Frequency Domain Analysis

The linearity or piece-wise linearity of each functional block in Fig. 1 over the useful UWB band allows modelling its input-output characteristics using the concept of frequency domain transfer function. Accordingly, the transfer function (between Points A and B in Fig. 1) is the multiplication of the MWP transfer function $H_{MWP}(\omega)$, the transfer function of the SMF $H_{SMF}(\omega)$ and the PD transfer function $H_{PD}(\omega)$ as follows:

$$\mathbf{H}_{opt}(\omega) = H_{MWP}(\omega).H_{SMF}(\omega).H_{PD}(\omega) \quad (3)$$

The electrical transfer function (between Points B and C in Fig. 1) is the multiplication of the PA transfer function $H_{PA}(\omega)$, the frequency response of the UWB TX antenna

$G_{TX}(\omega)$, the frequency response of the channel $H_{CH}(\omega)$, the frequency response of the UWB RX antenna $G_{RX}(\omega)$ and the transfer function of the LNA $H_{LNA}(\omega)$, written as follows:

$$\mathbf{H}_{elec}(\omega) = H_{PA}(\omega).G_{TX}(\omega).H_{CH}(\omega).G_{RX}(\omega).H_{LNA}(\omega) \tag{4}$$

The overall transfer function of the IR-UWBoF system with respect to the input basis function (between Points A and C in Fig. 1) is therefore given by the product of the optical and the electrical transfer functions as follows:

$$\mathbf{H}(\omega) = \mathbf{H}_{opt}(\omega) \times \mathbf{H}_{elec}(\omega) \tag{5}$$

Although the design of an IR-UWBoF system might aims at the generation of the k^{th} order derivative of the input basis function, some components in the IR-UWBoF system show additional, but unintended, time domain differentiation and/or integration effects. For example, the UWB TX and RX antennas act as differentiation elements due to their poor radiation efficiency at low frequencies (below ~1 GHz) [17]. In this context, it is assumed that the entire IR-UWBoF system is equivalent to an ideal m^{th} order time domain differentiator, where $k \neq m$ in general and m includes both the desired and the additional unintended differentiation effects. Accordingly, the overall system transfer function in (5) is decomposed as follows:

$$\mathbf{H}(j\omega) = A_n D(j\omega)\Pi(j\omega, \Theta) \tag{6}$$

where A_n is a normalization constant that accounts for the possible net gain/attenuation introduced by the entire IR-UWBoF system, $D(j\omega) = (j\omega)^m$ is the transfer function of an m^{th} order differentiator filter that models the combined differentiation and/or integration effects introduced by various system components, and $\Pi(j\omega, \Theta) \leq 1 \forall\ \omega$ denotes the residual non-ideality transfer function that remains after removing $D(j\omega)$ and A_n from $\mathbf{H}(j\omega)$, while $\Theta \in \mathbf{R}^N$ is a vector that contains all of the controllable parameters involved in the system design. Fig. 2 (b) illustrates the equivalent block diagram of the IR-UWBoF system shown in Fig. 1 (from Point A to Point C), based on (6).

Based on the decomposition of $\mathbf{H}(j\omega)$ in (6), the main goals of practical IR-UWBoF systems are explained as follows: The transfer function $D(j\omega)$ is applied to the input basis function such that an ideal m^{th} order IR-UWB waveform is produced. Since ideal derivatives of Gaussian and soliton basis functions are not inherently fully compliant to the FCC spectral mask, the net gain/attenuation, offered by the normalization constant A_n, adapts the peak PSD of the m^{th} order IR-UWB waveform to the maximum PSD admissible by the FCC spectral mask and is given by

$$A_n = \left(\frac{\max\{S_{FCC}(\omega)\}}{\max\left\{\left|\Psi^{(m)}(j\omega, \tau)\right|^2\right\}} \right)^{1/2}$$

where $S_{FCC}(\omega)$ is the FCC spectral mask, $\Psi^m(j\omega, \tau) = D(j\omega)\Psi(j\omega, \tau)$ and $\Psi(j\omega, \tau)$ is the Fourier transform of (2). Accordingly, the IR-UWB waveform at Point B in Fig. 2 is given by

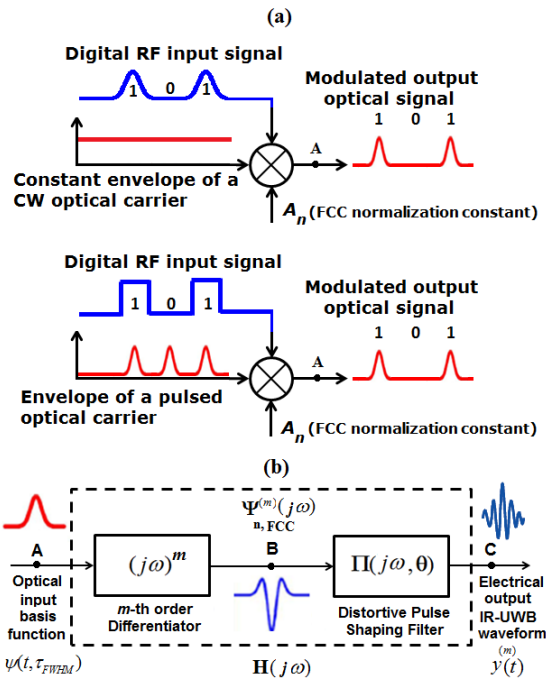

Fig. 2. Equivalent block diagram representation of the IR-UWBoF system depicted in Fig. 1. (a) equivalent block diagram representation of the optical modulator before point A in Fig. 1. (b): after point A. Red colors: optical waveforms. Blue colors: electrical waveforms.

$$\Psi^{(m)}_{n,FCC}(\omega) = \begin{cases} A_n(j\omega)^m \tau_g \sqrt{\pi} \exp\left(\frac{-(\omega\tau_g)^2}{2}\right) \\ A_n(j\omega)^m 4\pi\tau_s \mathrm{sech}(2\pi\omega\tau_s) \end{cases} \tag{7}$$

where $\Psi^{(m)}_{n,FCC}(j\omega, \tau)$ is the PSD of the m^{th} order derivative of the input basis function normalized to the maximum admissible FCC PSD. The role of the non-ideality transfer function $\Pi(j\omega, \Theta)$ is to reshape the spectrum of the m^{th} order IR-UWB waveform such that its compliance to the FCC spectral mask is achieved over entire spectrum. Thirdly, the IR-UWBoF system design is optimized by properly designing $\Pi(j\omega, \Theta)$ through the adjustment of the practically controllable parameters vector Θ such that the spectrum of the radiated IR-UWB waveform (at Point C in Fig. 2 (b)) is fully compliant with the FCC spectral constraints for all values of ω. However, the parameters set Θ does not include the parameters that can be controlled to adjust the FWHM pulse width τ of the input basis function. For simplicity, the transfer function $\Pi(j\omega, \Theta)$ is represented as an ideal passive bandpass filter (BPF) whose frequency response is centered at $\omega_o = (\omega_L + \omega_H)/2$ and is bounded by a lower and a higher cutoff frequencies of ω_{c_L} and ω_{c_H}, respectively. This is expressed mathematically as follows:

$$\Pi(j\omega, \Theta) = \begin{cases} 1; & \omega_{c_L} \leq \omega \leq \omega_{c_H} \\ 0; & \text{elsewhere} \end{cases} \tag{8}$$

where $\omega_{c_L} = \omega_o - \pi\Delta f, \omega_{c_H} = \omega_o + \pi\Delta f$ and $0 < \Delta f \leq (\omega_H - \omega_L)/2\pi$ is defined as the effective IR-UWBoF system bandwidth.

III. SPE Upper Bounds of Arbitrarily Filtered Gaussian and Soliton Based IR-UWB Waveforms: Problem Reformulation

The spectral power efficiency of a UWB signal is defined as the ratio of the power contained in its PSD in the useful UWB band to the total power admissible by the FCC mask within the same band [18]. Applying this definition to (7); the spectral power efficiency of the received IR-UWB waveform is expressed as follows:

$$\eta = \int_{\Omega} |\Psi^{(m)}_{n,FCC}(j\omega,\tau)|^2 |\Pi(j\omega,\Theta)|^2 d\omega / \int_{\Omega} S_{FCC}(\omega) d\omega \tag{9}$$

Subject to

$$\max\left\{|\Psi^{(m)}_{n,FCC}(j\omega,\tau)|^2 |\Pi(j\omega,\Theta)|^2\right\} \leq S_{FCC}(\omega) \forall \omega \tag{10}$$

where $\Omega \triangleq [\omega_L, \omega_H]$. Since $S_{FCC}(\omega) = \max\{S_{FCC}(\omega)\}\,\forall\omega \in [\omega_L, \omega_H]$, the SPE of (12) is given by

$$\eta = \frac{1}{\Omega} \int_{\Omega} |\Psi^{(m)}_{n}(j\omega,\tau)|^2 |\Pi(j\omega,\Theta)|^2 d\omega \tag{11}$$

where $|\Psi^{(m)}_{n}(j\omega)|^2 = |\Psi^{(m)}(j\omega,\tau)|^2 / \max\left\{|\Psi^{(m)}(j\omega,\tau)|^2\right\}$. The SPE in (9), or equivalently (11), is the objective function that constitute the main optimization problem of IR-UWBoF systems. The analytical solution of this joint optimization problem is an optimal parameter set $(\tau_{opt}, \Theta_{opt})$ which leads to an optimal IR-UWB waveform and system design, respectively. However, it is not always possible to obtain an analytical expression for η in a particular IR-UWBoF system unless every functional constituting block and component in this system is identified and its frequency response is given analytically. Unfortunately, this is not always possible due to a number of reasons. For example, the frequency response of the TX-RX antenna pair is often simulated or measured by a vector network analyzer (VNA) [17]. The problem of computing and optimizing the SPE in (11) is substantially simplified if the integrand is splitted into two independent integrands with each term worked on independently. Applying Cauchy-Schwarz-Holder inequality [19] to (11), the following inequality is obtained:

$$\eta \leq \left(\frac{1}{\Omega}\int_{\Omega} |\Psi^{(m)}_{n}(j\omega,\tau)|^4 d\omega\right)^{1/2} \left(\frac{1}{\Omega}\int_{\Omega} |\Pi(j\omega,\Theta)|^4 d\omega\right)^{1/2} \tag{12}$$

A direct consequence of applying Cauchy-Schwarz-Holder inequality is that an upper-bound for the SPE is obtained instead of its value that is not always computable from (11). This upper limit is the objective function that should be optimized, with each of its two terms worked on independently. Clearly, the joint optimization problem in (11) is simplified into two disjoint optimization problems that can be solved independently. Defining

$$\zeta^m(\tau) \triangleq \left(\frac{1}{\Omega}\int_{\Omega} |\Psi^{(m)}_{n}(j\omega,\tau)|^4 d\omega\right)^{1/2} \tag{13}$$

and

$$I(\Theta) \triangleq \left(\frac{1}{\Omega}\int_{\Omega} |\Pi(j\omega,\Theta)|^4 d\omega\right)^{1/2} \tag{14}$$

For an arbitrarily frequency dependent $\Pi(j\omega,\Theta)$, the SPE upper bound inequality in (12) is expressed, in terms of (13) and (14), as follows:

$$\eta \leq \zeta^m(\tau) I(\Theta) \tag{15}$$

From (15), it is observed that the value of $\zeta^{(m)}(\tau)$ depends on the pulse shape of the input basis function, its FWHM pulse width and the order of the derivative *m*, regardless of the particular system design parameters. Therefore, it can be defined as the upper bound of the SPE of the IR-UWB waveform, normalized to the functional $I(\Theta)$, which depends on the particular design of IR-UWBoF system. Hence, it is more useful to define a normalized SPE as follows:

$$\eta_{norm} \leq \zeta^m(\tau) \tag{16}$$

where $\eta_{norm} \triangleq \eta / I(\Theta)$. It should be noted that, based on the definition of $\Pi(j\omega,\Theta)$ in (8) as an ideal BPF, $I(\Theta) = 1$ and η_{norm} is equivalent to η in (16). Applying $\partial\Psi^{(m)}_{n,FCC}(j\omega,\tau)/\partial\omega = 0$ to (7) and solving for ω yields the peak emission frequency, denoted by ω_p. This frequency is substituted in $|\Psi^{(m)}(j\omega,\tau)|^2$ to obtain $\max\left\{|\Psi^{(m)}(j\omega,\tau)|^2\right\}$. For Gaussian-based IR-UWB waveforms, solving $\partial\Psi^{(m)}_{n,FCC}(j\omega,\tau)/\partial\omega = 0$ for ω results in a $\tau - \omega_p$ inverse proportionality relationship as [18]

$$\omega_{p,g} = \frac{\sqrt{2m}}{\tau_g} \tag{17}$$

where $\omega_{p,g}$ is the peak emission frequency of an m^{th}order Gaussian-based IR-UWB waveform. The peak emission frequency of an m^{th} order soliton-based IR-UWB waveform, denoted by $\omega_{p,s}$, results from using numerical solution techniques to solve the following transcendal equation:

$$2\pi\omega_{p,s}\tau_s \tanh(2\pi\omega_{p,s}\tau_s) = m \tag{18}$$

The normalization constant in (7) for the Gaussian and soliton-based IR-UWB waveforms is expressed, respectively, as follows:

$$A^m_g = \left(S_{FCC}(\omega)/\omega^{2m}_{p,g}\pi\tau^2_g \exp\left(-(\omega_{p,g}\tau_g)^2/2\right)\right)^{1/2} \tag{19}$$

$$A^m_s = \left(S_{FCC}(\omega)/\omega^{2m}_{p,s}(4\pi\tau_s)^2 \mathrm{sech}^2(2\pi\omega_{p,s}\tau_s)\right)^{1/2} \tag{20}$$

The upper bound of η_{norm} for Gaussian-based IR-UWB waveforms is obtained by substituting (7) and (19) in (13) as follows:

$$\zeta_g^m(\tau_g,\Delta f)=\left(\frac{(\pi\tau_g)^2}{\Omega G_p^2}\int_{(\omega_o-\pi\Delta f)\tau_g}^{(\omega_o+\pi\Delta f)\tau_g}\omega^{4m}\exp\left(-(\omega\tau_g)^2\right)d\omega\right)^{1/2} \quad (21)$$

where $G_p = \omega_{p,g}^m\tau_g\sqrt{\pi}\exp\left(-(\omega_{p,g}\tau_g)^2/2\right)$, while for soliton-based IR-UWB waveforms this upper bound is obtained from (13) in terms of (7) and (20) as follows:

$$\zeta_s^m(\tau_s,\Delta f)=\left(\frac{(4\pi\omega_p\tau_s)^4}{\Omega S_p^2}\int_{(\omega_o-\pi\Delta f)\tau_s}^{(\omega_o+\pi\Delta f)\tau_s}\omega^{4m}\mathrm{sech}^4(2\pi\omega\tau_s)d\omega\right)^{1/2} \quad (22)$$

where $S_p{=}4\pi\omega_{p,s}^m\tau_s\mathrm{sech}(2\pi\omega_{p,s}\tau_s)$. The integrals in (21) and (22) can be evaluated either analytically or by using numerical integration techniques. The closed form analytical solution of (21) yields:

$$\zeta_g^m(\tau_g,\Delta f)=\left(\frac{\pi^2\Gamma(2m+1/2)}{2\Omega G_p^2\tau_g^{4m-3}}\Big[\,erf(u)-\exp(-u^2)\times\sum_{n=0}^{2m-1}\frac{u^{4m-2n-1}}{\Gamma(2m-n+1/2)}\Big]_{(\omega_o-\pi\Delta f)\tau_g}^{(\omega_o+\pi\Delta f)\tau_g}\right)^{1/2} \quad (23)$$

where $[F(u)]_{u_1}^{u_2} \triangleq F(u_2)-F(u_1), \Gamma(z)$ is the gamma function given by $\Gamma(z)=\int_{x=0}^{\infty}y^{z-1}\exp(-y)dy$ and $erf(z)=(2/\sqrt{\pi})\int_0^z\exp(-y^2)dy$. Similarly, the closed analytical solution of the integral in (22) for soliton-based IR-UWB waveform yields

$$\zeta_s^m(\tau_s,\Delta f)=\left(\frac{(16\pi)^3}{2\Omega S_p^2\tau_s^{4m-3}}\left(\frac{4m!}{(2\pi)^{4m}}\right)[T(u)]_{u_L}^{u_H}\right)^{1/2} \quad (24)$$

where $u_H=2\pi(\omega_o+\pi\Delta f)\tau_s, u_L=2\pi(\omega_o-\pi\Delta f)\tau_s, T(u)$ is given by:

$$\mathrm{T(u)}=\sum_{q=0}^{4m}\sum_{l=0}^{K}\frac{(-1)^{l-1}(l+1)}{(4m-q)!(2l+4)^{q+1}}u^{4m-q}\exp\left(-2(l+2)u\right)$$

and $K\gg 1$. The higher the value of K is, the more accurate value of $T(u)$ is obtained. The optimal sets $(\tau_{g,opt}^m,\Delta f_{opt})$ and $(\tau_{s,opt}^m,\Delta f_{opt})$ can be obtained by applying either analytical or numerical optimization techniques to (23) and (24), respectively.

IV. Results and Analysis:Optimal Pulse widths, Bandwidths and Maximum Efficiency

This section provides numerical simulation results to quantify and optimize the analytical expressions in (23) and (24), derived in Section III. According to the FCC recommendations in [1], the useful UWB band is specified as follows: $f_L = 3.1$ GHz, $f_H = 10.6$ GHz and $\max\{S_{FCC}(\omega)\}$ = -41.3 dBm/MHz. Consequently, the frequency response of the BPF in (8) is centered at $f_o=(f_L+f_H)/2 = 6.85$ GHz and the effective system bandwidth Δf ranges from 0 to $f_H-f_L = 7.5$ GHz. The FWHM pulse width τ is varied from 0 to 500 ps for Gaussian-based IR-UWB waveforms and from 0 to 300 ps for soliton-based IR-UWB waveforms with a time resolution of 1 ps. The derivative order *m* takes values through $\{1,2,...7\}$.

The simulation starts by evaluating the values of τ_g and τ_s corresponding to each value of the FWHM pulse width τ . The values of τ_g and τ_s are then used in calculating the peak emission frequencies $\omega_{p,g}$ and $\omega_{p,s}$ in (17) and (18) as well as the corresponding normalization constants in (19) and (20), respectively. These parameters are used in evaluating the integrals in (21) and (22) by using the trapezoidal numerical integration technique as well as their corresponding closed form analytical expressions in (23) and (24), respectively.

Fig. 3 (a) shows the set of achievable upper bounds of $\eta_{norm}$with Gaussian-based IR-UWB waveforms for different values of *m* and τ and an effective system bandwidth of 7.5 GHz. Fig. 3 (b) shows the corresponding set (with the same values of *m* and Δf) for soliton-based IR-UWB waveforms. Both figures show that the analytically obtained results exactly match those obtained by numerical integration, which indicates the accuracy of the proposed closed form expressions in (23) and (24). Furthermore, for each waveform type and order *m*, there exists an optimum FWHM pulse width of the input basis function at which the SPE upper bound attains a global optimum. The higher is the pulse order *m*, the higher is its optimum FWHM pulse width and the lower is its global optimum SPE point. This is explained as follows. Due to the inverse relationship between the FWHM pulse width and the peak emission frequency, the PSDs of IR-UWB waveforms with small FWHM pulse widths are concentrated at frequencies much higher than the useful UWB window. The higher is the FWHM pulse width of an IR-UWB waveform, the lower is its peak emission frequency and the more is its PSD shifted towards low frequencies until it enters the useful UWB band. Increasing the derivative order *m* of the IR-UWB waveform has the same effect on its spectrum as increasing its peak emission frequency as both lead to shifting its PSD towards higher frequencies.

A close inspection in both figures indicates that the value of ${\zeta_s}^m$ for a given m^{th}order soliton-based IR-UWB waveform is always larger than ${\zeta_g}^m$ of its Gaussian-based counterpart of the same order and FWHM pulse width τ. For example, the maximum SPE of a Gaussian monocycles is upper bounded by 84.72%, while the maximum SPE of a soliton monocycle is upper bounded by 87.6%. Although the difference is not quite large for all values of *m*, the values of ${\zeta_s}^m$decrease more rapidly with τ for soliton-based IR-UWB waveforms than ${\zeta_g}^m$ for their Gaussian-based counterparts. Consequently, the SPE optimal values of soliton-based IR-UWB waveforms are achieved at FWHM pulse widths much smaller than with Gaussian-based IR-UWB waveforms. This is still an advantage since small pulse widths are always desirable in high bit rate IR-UWBoF systems.

Another interesting observation in Fig. 3 (a) is that, among all Gaussian-based IR-UWB waveforms, the highest upper

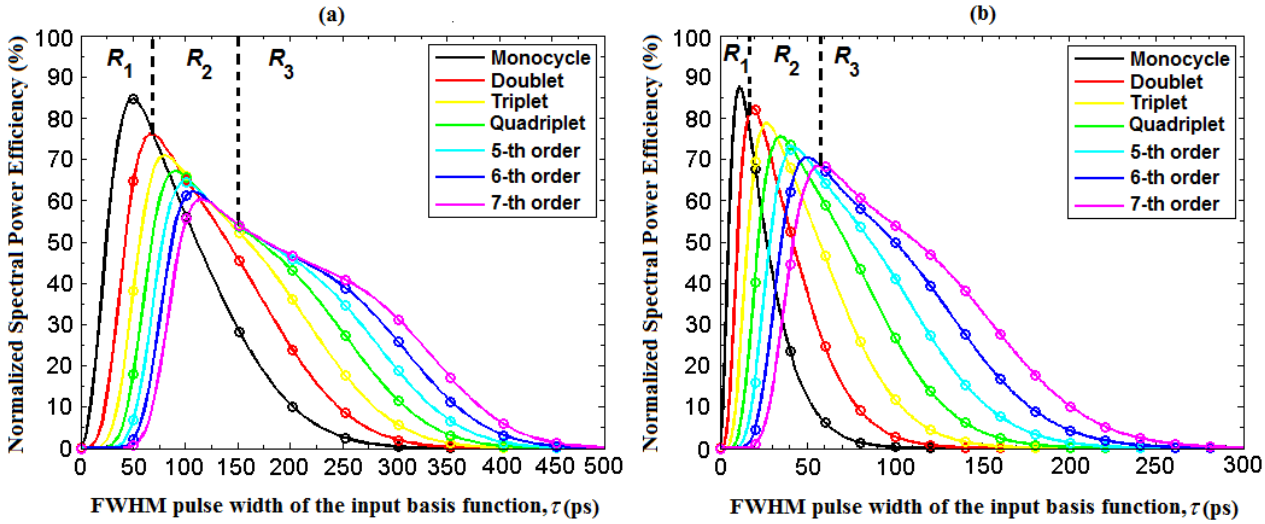

Fig. 3. Normalized upper bounds for the spectral power efficiency versus the FWHM pulse width of (a): the Gaussian input basis function and (b): the soliton input basis function with Δf= 7.5 GHz. Solid lines: theoretically obtained expressions. Markers: results obtained from numerical integration. R_1 : Region 1; ${\zeta_g}^{(m)}(\tau) > {\zeta_g}^{(n)}(\tau) | m < n$. R_2 : Region 2; ${\zeta_g}^{(m)}(\tau) \gtreqless {\zeta_g}^{(n)}(\tau) | m \neq n$.$R_3$: Region 3; ${\zeta_g}^{(m)}(\tau) > {\zeta_g}^{(n)}(\tau) | m > n$.

bound of η_{norm} is achieved by the Gaussian monocycle pulse. Likewise, the soliton monocycle has the highest upper bound of η_{norm} among soliton based doublets, triplets and other higher order derivatives of the soliton input basis function. Nevertheless, this interesting feature explains why the monocycle pulse, regardless of its basis function, is the most preferred and popular among other IR-UWB waveforms in most of the literature published on the photonic generation of IR-UWB waveforms and adds an extra advantage to the monocycle pulse besides its ease of photonic generation and superior BER performance in dense multipath fading wireless channels [20]. However, the superiority of monocycle pulses is not guaranteed over the whole range of τ.

A closer inspection in both figures reveals that, for each waveform type it is more useful to view the whole range of τ as composed of three sub-ranges: R_1, R_2 and R_3. For FWHM pulse widths in R_1, corresponding to $0 \leq \tau \leq 70.72$ ps for Gaussian input basis functions and $0 \leq \tau \leq 16.06$ ps for soliton input basis functions, ${\zeta_g}^{(m)}(\tau) > {\zeta_g}^{(n)}(\tau) | m < n$. Within R_2, corresponding to $70.72 < \tau \leq 136.4$ ps for Gaussian input basis functions and $16.06 < \tau \leq 57.2$ ps for soliton input basis functions, the superiority of an m^{th} order IR-UWB waveform over another n^{th} order waveform of the same type and FWHM pulse width τ depends on the particular values of *m*, *n* and τ, where ${\zeta_g}^{(m)}(\tau) \gtreqless {\zeta_g}^{(n)}(\tau)$ and ${\zeta_s}^{(m)}(\tau) \gtreqless {\zeta_s}^{(n)}(\tau)$ for $m \neq n$.

For the third range R_3, corresponding to $136.4 < \tau$ ps for Gaussian input basis functions and $57.2 < \tau$ ps for soliton input basis functions, the situation is opposite to that in R_1 and the SPE of an n^{th} order IR-UWB waveform is larger than that of an m^{th} one having the same pulse width, $m < n$.

V. Conclusion

In this work, the problem of optimal IR-UWB waveform design in IR-UWBoF systems with combined optical and wireless transmission is reformulated, considering two common IR-UWB waveform types. Accurate closed form analytical expressions for the upper bounds of the spectral power efficiency of these waveforms are derived. A powerful advantage of the provided analysis is that it can be generalized and applied to many of the IR-UWB waveforms available in the literature on IR-UWBoF systems.

References

[1] "First report and order, (Revision of part 15 of the commission's rules regarding ultra-wideband transmission systems), US. Fed. Comm. Commission, adopted Feb. 14, 2002, released Apr. 22, 2002." Tech. Rep.

[2] M. G. Di Benedetto and B. Vojcic, "Ultra-wideband wireless communications: A Tutorial," J. Commun. Netw., vol. 5, no. 4, pp 290-302, Dec. 2003.

[3] Tianye Huang; Jia Li; Sun, Junqiang; Chen, L.R., "Photonic Generation of UWB Pulses Using a Nonlinear Optical Loop Mirror and Its Distribution Over a Fiber Link," in Photonics Technology Letters, IEEE , vol.23, no.17, pp.1255-1257, Sept.1, 2011.

[4] Bowen Luo; Jianji Dong; Xinliang Zhang, "Photonic generation of UWB doublet pulse based on XPM in an SOA-based NOLM," in Opto-Electronics and Communications Conference (OECC), 2012 17th , vol., no., pp.717-718, 2-6 July 2012.

[5] Luo Bo-Wen,"Photonic multi-shape UWB pulse generation using a semiconductor optical amplifier-based nonlinear optical loop mirror ", Chin. Phys. B., vol. 22, no. 5, pp. 1-5, Dec. 2013.

[6] Hanlin Feng; Fok, M.P.; Shilin Xiao; Jia Ge; Qi Zhou; Locke, M.; Toole, R.; Weisheng Hu, "A Reconfigurable High-Order UWB Signal Generation Scheme Using RSOA-MZI Structure," in Photonics Journal, IEEE , vol.6, no.2, pp.1-7, April 2014.

[7] You Min Chang; Junsu Lee; Haeng-Seon Lee; Lianshan Yan; Ju Han Lee, "Generation and Distribution of 1.25 Gb/s Ultrawideband Doublet Pulses Based on the Combination of Nonlinear Polarization Rotation and Parametric Amplification," in Lightwave Technology, Journal of , vol.29, no.6, pp.931-938, March15, 2011.

[8] Junsu Lee; You Min Chang; Ju Han Lee, "UWB doublet pulse generation using the combination of parametric amplification and cross phase modulation," in Photonics Conference (IPC), 2012 IEEE , vol., no., pp.584-585, 23-27 Sept. 2012.

[9] Zadok, A.; Xiaoxia Wu; Sendowski, J.; Yariv, A.; Willner, A.E., "Reconfigurable Generation of High-Order Ultra-Wideband Waveforms Using Edge Detection," in Lightwave Technology, Journal of , vol.28, no.16, pp.2207-2212, Aug.15, 2010.

[10] Abtahi, M.; Magne, J.; Mirshafiei, M.; Rusch, L.A.; LaRochelle, S., "Generation of Power-Efficient FCC-Compliant UWB Waveforms Using FBGs: Analysis and Experiment," in Lightwave Technology, Journal of, vol.26, no.5, pp.628-635, March1, 2008.
[11] P. Li, H. Chen, M. Chen, S. Xie "Gigabit/s Photonic Generation, Modulation, and Transmission for a Reconfigurable Impulse Radio UWB over Fiber System", IEEE Photonics Journal, vol.4, no.3, 2012.
[12] P. Li, H. Chen, X. Wang, H. Yu, M. Chen, S. Xie "Photonic Generation and Transmission of 2-Gbit/s Power-Efficient IR-UWB Signals Employing and Electro-Optic Phase Modulator" IEEE Photonics Technology Letters, vol.25, no.2, 2013.
[13] Chao Wang; Fei Zeng; Jianping Yao, "All-Fiber Ultrawideband Pulse Generation Based on Spectral Shaping and Dispersion-Induced Frequency-to-Time Conversion," in Photonics Technology Letters, IEEE , vol.19, no.3, pp.137-139, Feb.1, 2007.
[14] Li, Jia; Kuo, B.P.-P.; Wong, Kenneth Kin-Yip, "Ultra-Wideband Pulse Generation Based on Cross-Gain Modulation in Fiber Optical Parametric Amplifier," in Photonics Technology Letters, IEEE , vol.21, no.4, pp.212-214, Feb.15, 2009.
[15] Junsu Lee; You Min Chang; Ju Han Lee, "UWB doublet pulse generation using the combination of parametric amplification and cross phase modulation," in Photonics Conference (IPC), 2012 IEEE , vol., no., pp.584-585, 23-27 Sept. 2012.
[16] M. Ghavami, L. B. Michal, and R. Kohno, Ultra Wide Band Signals and Systems in Communication Engineering." West Sussex, England: Wiley, 2007.
[17] Mirshafiei, M.; Abtahi, M.; Larochelle, P.; Rusch, L.A., "Pulse Shapes That Outperform Traditional UWB Antenna/Waveform Combinations," in Global Telecommunications Conference (GLOBECOM 2010), 2010 IEEE , vol., no., pp.1-5, 6-10 Dec. 2010.
[18] S. T. Abraha, C. Okonkwo, H. Yang, D. Visani, Y. Shi, H.-D. Jung, E. Tangdiongga, and T.Koonen, "Performance evaluation of IR-UWB in short-range fiber communication using linear combination of monocycles," J. Lightwave Technol., vol. 29, no. 8, pp. 1143-1151, Apr. 2011.
[19] Carlos Finol and Marek Wojtowicz, "Cauchy-Schwarz and Holder's inequalities are equivalent," in Divulgaciones Matematicas, vol.15, no.2, pp.143-147, 2007.
[20] X. Chen and S. Kiaei, "Monocycle shapes for ultra wideband system," in IEEE Int. Symp. Circuits Syst., May 2002, vol. 1, pp. 26-29

Mohamed Shehata (M'11) received the B.Sc. and M. Sc. degrees in electronics and communications engineering from Al-Azhar University, Cairo, Egypt, in 2006 and 2012, respectively. He is currently working toward the PhD degree in electrical engineering with the Department of Electronics and Communications Engineering, Cairo University. He is currently a Research Assistant with the Opto-Nano-Electronics (ONE) laboratory, Electronics and Communications Department, Cairo University. His research interests include, but not limited to, microwave photonics, radio over fiber communications, tribo-phototronics.

Hassan Mostafa (S'01-M'11-SM'15) received the B.Sc. and M.A.Sc. degrees (Hons.) in electronics engineering from Cairo University, Cairo, Egypt, in 2001 and 2005, respectively, and the Ph.D. degree in electrical and computer engineering from the Department of Electrical and Computer Engineering, University of Waterloo, Waterloo, ON, Canada, in 2011.

He is currently an Assistant Professor with the Electronics and Communications Department, Cairo University, and also an Adjunct Assistant Professor with the Center for Nano-Electronics and Devices, American University in Cairo, Cairo. He has worked as an Natural Sciences and Engineering Research Council of Canada (NSERC) Post-Doctoral Fellow with the Department of Electrical and Computer Engineering, University of Toronto, Toronto, ON, Canada. His Post-Doctoral Research includes the design of the next generation FPGA in collaboration with Fujitsu Research Laboratory, Japan/USA. He is collaborating with several sponsors across the world such as Intel, USA, Fujitsu, Japan, National Telecommunications Regulation Agency, Egypt, the University of Toronto, the University of Waterloo, the Academy of Scientific Research and Technology, Egypt, NSERC, Cairo University, Blackberry, Canada, Qatar National Research Fund, Qatar. He has authored/coauthored over 80 papers in international journals and conferences and published four books. His research interests include analog-to-digital converters, low-power circuits, subthreshold logic, variation-tolerant design, soft error tolerant design, statistical design methodologies, next generation FPGA, spintronics, memristors, energy harvesting MEMS/NEMS, power management, and opto-electronics. Dr. Mostafa was a recipient of the University of Toronto Research Associate Scholarship in 2012, the NESRC Prestigious Post-Doctoral Fellowship in 2011, the Waterloo Institute of Nano-Technology Nanofellowship Research Excellence Award in 2010, the Ontario Graduate Scholarship in 2009, and the University of Waterloo SandFord Fleming TA Excellence Award in 2008.

Yehea Ismail (F'13) is the Director of the Nano-electronics and Devices Center, Zewail City and the American University in Cairo. He is an Editor-in-Chief of the IEEE TRANSACTIONS ON VERY LARGE SCALE INTEGRATION (VLSI) SYSTEMS and the Chair Elect of the IEEE VLSI technical committee. He is on the Editorial Board of the Journal of Circuits, Systems, and Computers, was on the Editorial Board of the IEEE TRANSACTIONS ON CIRCUITS AND SYSTEMS I: FUNDAMENTAL THEORY AND APPLICATIONS, and the Guest Editor for a special issue of the IEEE TRANSACTIONS ON VERY LARGE SCALE INTEGRATION (VLSI) SYSTEMS on SOn-Chip Inductance in High Speed Integrated Circuits. T He has also chaired many conferences such as GLSVLSI, IWSOC, and ISCAS. He is the Chief Scientist of the Innovation and Entrepreneurship Center of the Ministry of Communications and Information Technology, Egypt. Prof. Ismail was a recipient of several awards such as the USA National Science Foundation Career Award, the IEEE CAS Outstanding Author Award, the Best Teacher Award at Northwestern University, and many other best teaching awards and best paper awards. He is the Distinguished Lecturer of the IEEE CASS. He has published over 170 papers in top refereed journals and conferences and many patents. He has co-authored three books entitles On-Chip Inductance in High Speed Integrated Circuits, Handbook on Algorithms for VLSI Physical Design, and Temperature-Aware Computer Architecture. He has many patents in the area of high performance circuits and interconnect design and modeling. His work is some of the most highly cited in the very large scale integration area and is extensively used by industry.